Theoretical treatment of charge transfer in collisions of C^{2+} ions with HF: Anisotropic and vibrational effect

E. Rozsályi,[1] E. Bene,[2] G. J. Halász,[3] Á. Vibók,[1] and M. C. Bacchus-Montabonel[4]

[1]*Department of Theoretical Physics, University of Debrecen, Post Office Box 5, H-4010 Debrecen, Hungary*
[2]*Institute of Nuclear Research, Hungarian Academy of Sciences, Post Office Box 51, H-4001 Debrecen, Hungary*
[3]*Department of Information Technology, University of Debrecen, Post Office Box 12, H-4010 Debrecen, Hungary*
[4]*Laboratoire de Spectrométrie Ionique et Moléculaire, Université de Lyon I, CNRS UMR 5579,*
43 Boulevard du 11 Novembre 1918, F-69622 Villeurbanne Cedex, France

The charge transfer in collisions of C^{2+} ions with the HF molecule has been studied by means of *ab initio* quantum chemistry molecular methods followed by a semiclassical dynamical treatment in the keV collision energy range. The mechanism of the process, in particular its anisotropy, has been investigated in detail in connection with nonadiabatic interactions around avoided crossings between states involved in the reaction. The vibration of the molecular target has been analyzed and cross sections on different vibrational levels of HF^+ have been estimated in the Franck-Condon approximation.

PACS number(s): 34.70.+e

I. INTRODUCTION

Collisions of slow multiply charged ions with molecular species have been widely investigated in the past few years. Such studies give detailed information on electron capture processes occurring during the collision and fragmentation dynamics after removal of electrons from the target. Important experimental and theoretical effort has been focused on reactions with simple targets, such as H_2 or D_2 [1–4]. Consideration of more complex molecular targets are now of increasing interest [5–9], in particular with regard to possible direct or indirect processes occurring in the irradiation of the biological medium. Effectively, important damage induced by the interaction of ionizing radiation with biological tissues is due to the secondary particles, low-energy electrons, radicals, or singly and multiply charged ions generated along the track after irradiation of the biological medium [10]. Experimental and theoretical studies have thus been developed on collisions between ions and molecular or even biomolecular targets [5–9,11–14] in order to understand the different mechanisms involved at the molecular level.

Experimental investigations of charge transfer in collisions with hydrogen chloride have been recently performed [11]. We have thus undertaken a theoretical study of such processes with hydrogen chloride and hydrogen fluoride targets. In a first step, we have studied the charge-transfer reaction in collisions of C^{2+} ions with the HF molecular target. Such a system may be compared to the previous C^{2+} + OH and C^{2+} + CO collision systems in order to extract some general rules on the mechanism of such processes. We are interested in particular in the anisotropy of the charge transfer with regard to the orientation of the projectile toward the target as well as in a detailed vibration analysis of the capture in the C^{2+} + HF($\nu = 0$) → C^+ + $HF^+(\nu)$ reaction. The equivalent process with the heavier HCl target is investigated later. The molecular calculation is performed using *ab initio* quantum chemistry methods in order to determine potential energy surfaces of the different states involved in the process and corresponding radial and rotational couplings. Semiclassical approaches are used for the collision dynamics.

II. MOLECULAR CALCULATIONS

The molecular calculations have been performed by means of the MOLPRO suite of *ab initio* programs [15] using state-averaged complete active space self-consistent field (CASSCF) multireference configuration interaction (MRCI) methods and the correlation-consistent triple-ζ aug-cc-pVTZ basis set of Dunning [16]. The active space includes the $n = 2$ and $n = 3(sp)$ orbitals for carbon and fluorine, and the $1s$ orbital for hydrogen. The $1s$ orbitals of carbon and fluorine have been frozen in the calculation. The optimized geometry of the $^1\Sigma^+$ ground state of HF is $r_{HF} = 1.73836832$ a.u. corresponding to a vertical ionization potential of 16.12 eV, in excellent agreement with the 16.1 eV experimental value [17–19] and previous calculations [20,21]. As shown in Table I, such an approach leads to a good agreement with separated species calculations taking account of experimental data for carbon ions [22] and ionization potential of the HF molecule [17,18] with MRCI calculations at optimized equilibrium geometry for the ground and excited states of the target molecule.

The geometry of the system may be described by the internal Jacobi coordinates $\{R, r_{HF}, \alpha\}$ with the origin at the center of mass of the target molecule, as defined in Fig. 1 such that, in the linear approach, the collision of the C^{2+} ion with hydrogen would correspond to the angle $\alpha = 0°$ and the collision with fluorine to the geometry $\alpha = 180°$, respectively. In order to study the anisotropy of the process, a series of calculations have been performed for different orientations of the projectile corresponding to specific values of the angle α, about every $20°$, from the linear C-H-F geometry ($\alpha = 0°$) to the linear C-F-H one ($\alpha = 180°$). In such linear geometries, the molecular calculations have been performed in the C_{2v} symmetry group. In contrast, for nonlinear geometries, the calculation has been carried out using the C_s symmetry group and considering the plane of the molecular system as the plane of symmetry. Spin-orbit coupling being negligible in the energy range of interest, electron spin may be conserved in the collision process and only singlet states may be correlated to the $^1\Sigma^+$ entry channel.

TABLE I. Comparison of asymptotic energies (in eV) from separated species at the optimized HF($^1\Sigma^+$) distance $R = 1.73836832$ a.u.

Configuration	This calculation	Separated species
$C^{2+}(^1S) + HF(^1\Sigma^+)$	8.368	8.279
$C^+(^2P) + HF^+(^2\Sigma^+)$	3.824	3.909
$C^+(^2P) + HF^+(^2\Pi)$	0	0

The charge-transfer process is driven mainly by nonadiabatic interactions in the vicinity of avoided crossings [23]. The radial coupling matrix elements between all pairs of states of the same symmetry have thus been calculated by means of the finite-difference technique:

$$g_{KL}(R) = \langle \psi_K | \partial/\partial R | \psi_L \rangle$$
$$= \langle \psi_K(R) | \lim_{\Delta \to 0} \frac{1}{\Delta} | \psi_L(R + \Delta) - \psi_L(R) \rangle,$$

which, taking into account the orthogonality of the eigenfunctions $|\psi_K(R)\rangle$ and $|\psi_L(R)\rangle$ for $K \neq L$, reduces to

$$g_{KL}(R) = \langle \psi_K | \partial/\partial R | \psi_L \rangle = \lim_{\Delta \to 0} \frac{1}{\Delta} \langle \psi_K(R) | \psi_L(R + \Delta) \rangle.$$

The parameter Δ has been tested and a value of $\Delta = 0.0012$ a.u. has been chosen as in previous calculations [24] using the three-point numerical differentiation method for reasons of numerical accuracy.

The interaction between $^1\Sigma^+$ and $^1\Pi$ states by means of rotational coupling has also been taken into account. The rotational coupling matrix elements $\langle \psi_K(R) | i L_y | \psi_L(R) \rangle$ between states of angular moment $\Delta\Lambda = \pm 1$ have been calculated directly from the quadrupole moment tensor from the expression $i L_y = x \frac{\partial}{\partial z} - z \frac{\partial}{\partial x}$ with the center of mass of the system as the origin of electronic coordinates.

A number of states may be considered with regard to the respective ionization potentials and different excited states of HF$^+$ and C$^+$ ions [21,22]:

$$C^{2+}(1s^22s^2)\,^1S + HF(^1\Sigma^+) \qquad ^1\Sigma^+,$$
$$C^+(1s^22s^22p)\,^4P + HF^+(^2\Pi) \qquad ^{3,5}\Sigma^+, ^{3,5}\Pi, ^{3,5}\Delta,$$
$$C^+(1s^22s^22p)\,^2P + HF^+(^2\Sigma^+) \qquad ^{1,3}\Sigma^+, ^{1,3}\Pi,$$
$$C^+(1s^22s^22p)\,^2P + HF^+(^2\Pi) \qquad ^{1,3}\Sigma^+, ^{1,3}\Pi, ^{1,3}\Delta.$$

Taking account of the $^1\Sigma^+$ symmetry of the $C^{2+}(1s^22s^2)^1S + HF(^1\Sigma^+)$ entry channel, only doublet C$^+$ excited states could be involved in the collision process. Besides, only $^1\Pi$ states could be correlated to the $^1\Sigma^+$ entry channel by
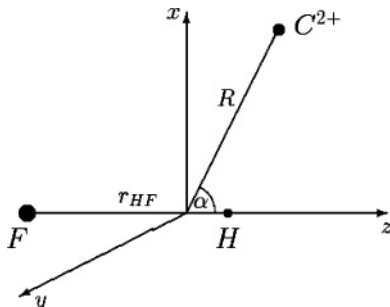

FIG. 1. Internal coordinates for the C^{2+}-HF collision system.

means of rotational coupling interaction. Three $^1\Sigma^+$ states and two $^1\Pi$ states must thus be considered in this process with regard to the different excited states of HF$^+$ and spin considerations:

$$C^{2+}(1s^22s^2)\,^1S + HF(^1\Sigma^+) \qquad ^1\Sigma^+,$$
$$C^+(1s^22s^22p)\,^2P + HF^+(^2\Sigma^+) \quad ^1\Sigma^+, ^1\Pi,$$
$$C^+(1s^22s^22p)\,^2P + HF^+(^2\Pi) \qquad ^1\Sigma^+, ^1\Pi$$

The potential energy curves for the equilibrium distance and associated radial and rotational coupling matrix elements between $^1\Sigma^+$ and $^1\Pi$ states have been calculated in the 2.0–14.0 a.u. internuclear distance range. The main features of the process may be clearly visualized in the molecular results for the collinear approach of the C^{2+} ion toward the HF target. The potentials for the angle $\alpha = 0°$ corresponding to a collision with the hydrogen atom are presented in Fig. 2(a). The $^1\Sigma^+$ states clearly show two avoided crossings, a smooth one at this geometry between the entry channel and the $2\,^1\Sigma^+\{C^+(1s^22s^22p)\,^2P + HF^+(^2\Sigma^+)\}$ exit channel around 6.5 a.u. and a sharper one, at shorter range, around $R = 4.5$ a.u., between the $2\,^1\Sigma^+$ and $1\,^1\Sigma^+\{C^+(1s^22s^22p)\,^2P + HF^+(^2\Pi)\}$ exit channels. These interactions correspond to peaks of the radial coupling matrix elements which may be visualized in Fig. 2(b). In contrast, $^1\Pi$ channels do not present significant avoided crossing in the distance range of interest; they interact only in the repulsive part of the potential energy curves. The rotational coupling matrix elements are presented in Fig. 2(c). Rotational coupling matrix elements between $^1\Pi$ states and the entry channel, or between $^1\Pi$ states and the $2\,^1\Sigma^+\{C^+(1s^22s^22p)\,^2P + HF^+(^2\Sigma^+)\}$ exit channel, vary abruptly in correspondence with the avoided crossing around 6.5 a.u. Effectively, the corresponding change of character of the $^1\Sigma^+$ wave functions in this region induces strong variation on rotational coupling matrix elements. In contrast, low interaction is observable between the lowest $1^1\Sigma^+\{C^+(1s^22s^22p)\,^2P + HF^+(^2\Pi)\}$ state and the entry channel and corresponding rotational couplings rot11 and rot21 remain rather unchanged. It is interesting to point out the similar behavior of rotational coupling matrix elements for $1\,^1\Pi$ and $2^1\Pi$ states in the linear geometry. In the C_{2v} symmetry group, they are described by the same configurations. This is no more the case for nonlinear geometries in C_s symmetry and rotational couplings between $^1\Sigma^+$ and $^1\Pi$ states correlated to different molecular states are becoming zero, as shown in Fig. 3(b) for the perpendicular geometry.

A strong evolution may be noticed on the potential energy curves when the angle α increases from the linear geometry $\alpha = 0°$ to nonlinear geometries, up to $\alpha = 90°$. The avoided crossing between the entry channel and the $2\,^1\Sigma^+$ level becomes sharper and moves toward shorter internuclear distances. On the other hand, the avoided crossing between $2\,^1\Sigma^+$ and $1\,^1\Sigma^+$ exit channels becomes smoother, as clearly shown in the potential energy curves in perpendicular geometry presented in Fig. 3(a). The evolution is inverse when the angle α increases still up to 180° in the linear C-F-H geometry. Nevertheless, the nonadiabatic interaction between the entry channel and the $2^1\Sigma^+$ level remains sharper in this half-plane, where the C^{2+} ion collides with the fluorine atom.
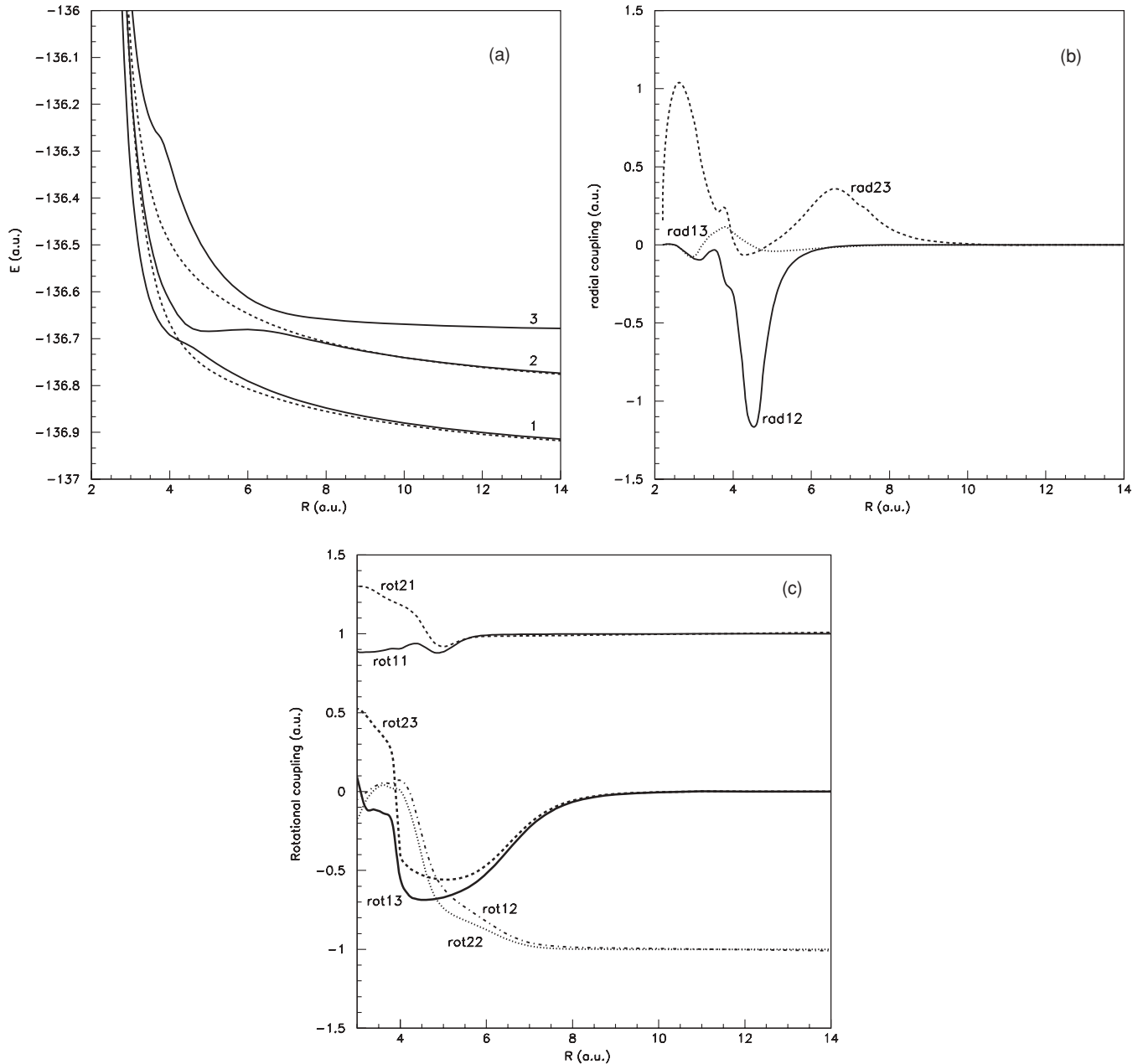
FIG. 2. (a) Potential energy curves for the $^1\Sigma^+$ (solid line) and $^1\Pi$ (dashed line) states of the C^{2+}-HF molecular system at equilibrium, $\alpha = 0°$: curve 1, $C^+(1s^22s^22p)\,^2P + HF^+(^2\Pi)$; curve 2, $C^+(1s^22s^22p)\,^2P + HF^+(^2\Sigma^+)$; curve 3, $C^{2+}(1s^22s^2)\,^1S + HF(^1\Sigma^+)$ entry channel. (b) Radial coupling matrix elements between $^1\Sigma^+$ states of the C^{2+}-HF molecular system at equilibrium, $\alpha = 0°$ [same labels as in part (a)]. (c) Rotational coupling matrix elements between $^1\Sigma^+$ and $^1\Pi$ states for the C^{2+}-HF molecular system at equilibrium, $\alpha = 0°$ [same labels as in part (a)]: rot11 $= \langle 1^1\Pi | iLy | 1^1\Sigma^+ \rangle$, rot12 $= \langle 1^1\Pi | iLy | 2^1\Sigma^+ \rangle$, rot13 $= \langle 1^1\Pi | iLy | 3^1\Sigma^+ \rangle$, rot21 $= \langle 2^1\Pi | iLy | 1^1\Sigma^+ \rangle$, rot22 $= \langle 2^1\Pi | iLy | 2^1\Sigma^+ \rangle$, rot23 $= \langle 2^1\Pi | iLy | 3^1\Sigma^+ \rangle$.

III. COLLISION DYNAMICS

The collision dynamics was performed by means of the EIKONX code [25] in the keV laboratory energy range. As straight-line trajectories are satisfying for energies higher than 10 eV/amu [26], semiclassical approaches may be used with good accuracy in this collision energy range. Because electronic transitions are much faster than vibrational and rotational motion, the sudden approximation may be used and cross sections, corresponding to purely electronic transitions, are determined by solving the impact-parameter equation as

in the usual ion-atom approach, considering the internuclear distance of the molecular target fixed in a given geometry. This relatively crude approach is widely used in the field of ion-molecule collisions and has shown its efficiency in the keV energy range dealt with in this paper [27].

This treatment was performed for different geometries of the C^{2+}-HF collision system, taking account of all the transitions driven by radial and rotational coupling matrix elements. The introduction of translation factors necessary for the cross sections to be independent of the origin of coordinates
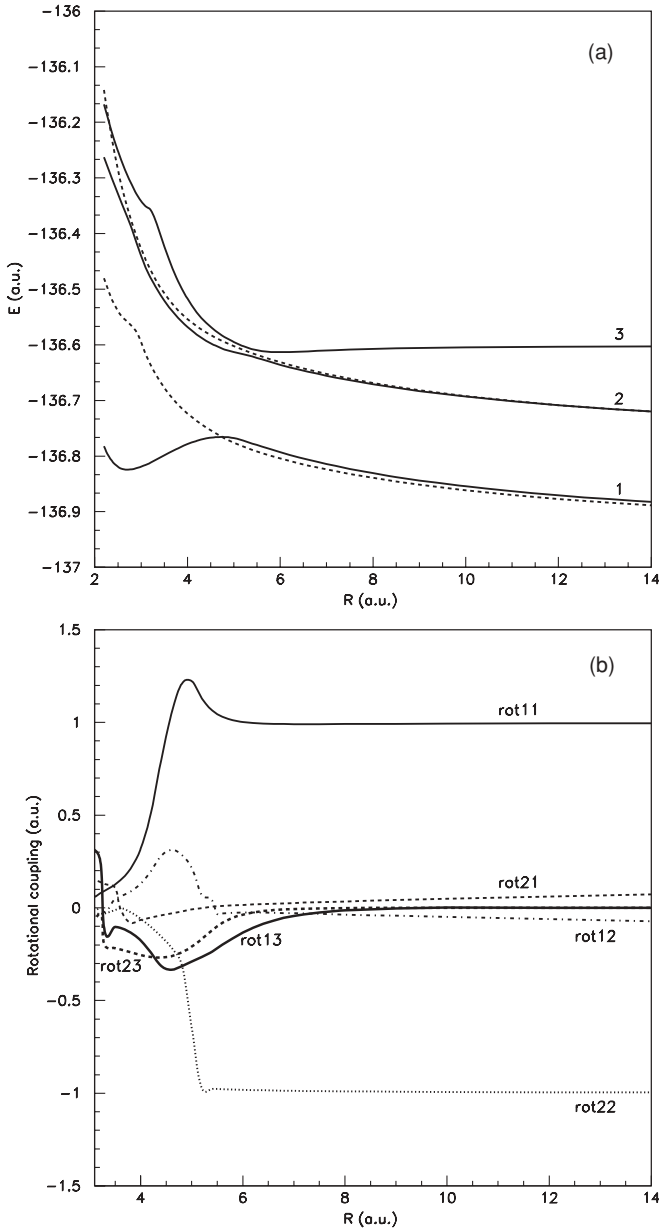
FIG. 3. (a) Potential energy curves for the $^1\Sigma^+$ (solid line) and $^1\Pi$ (dashed line) states of the C^{2+}-HF molecular system at equilibrium, $\alpha = 90°$: curve 1, $C^+(1s^22s^22p)\,^2P + HF^+(^2\Pi)$; curve 2, $C^+(1s^22s^22p)\,^2P + HF^+(^2\Sigma^+)$; curve 3, $C^{2+}(1s^22s^2)\,^1S + HF(^1\Sigma^+)$ entry channel. (b) Rotational coupling matrix elements between $^1\Sigma^+$ and $^1\Pi$ states for the C^{2+}-HF molecular system at equilibrium, $\alpha = 90°$ [same labels as in part (a)]: rot11 $= \langle 1^1\Pi|iLy|1^1\Sigma^+\rangle$, rot12 $= \langle 1^1\Pi|iLy|2^1\Sigma^+\rangle$, rot13 $= \langle 1^1\Pi|iLy|3^1\Sigma^+\rangle$, rot21 $= \langle 2^1\Pi|iLy|1^1\Sigma^+\rangle$, rot22 $= \langle 2^1\Pi|iLy|2^1\Sigma^+\rangle$, rot23 $= \langle 2^1\Pi|iLy|3^1\Sigma^+\rangle$.

and to avoid spurious coupling terms at long range has not been included in this study. However, the chosen origin coordinate may be expected to provide accurate enough values of total cross sections for impact velocities lower than 0.5 a.u. ($E_{lab} = 75$ keV) [27,28], even if transitions driven by rotational couplings could be slightly overestimated. Such a translation effect may be evaluated in the approximation of the common translation factors [29,30]. The radial and rotational coupling

matrix elements are thus transformed, respectively, into

$$\langle \psi_K|\partial/\partial R - (\varepsilon_K - \varepsilon_L)z^2/2R|\psi_L\rangle$$

and

$$\langle \psi_K|iL_y + (\varepsilon_K - \varepsilon_L)zx|\psi_L\rangle,$$

where ε_K and ε_L are the electronic energies of states $|\psi_K\rangle$ and $|\psi_L\rangle$, and z^2 and zx are the components of the quadrupole moment tensor. In this approach, the translation effect has been shown to be almost negligible for collision energies lower than 100 keV, even for long-range rotational couplings [31]. Such an effect depends, of course, on the collision system, but in a first approach we could consider that translation effects would be weak in the energy range we are dealing with. The partial and total cross sections have been calculated between the different quasimolecular states involved in the process. They would have to be projected on a fixed frame in order to be compared to experiment. Such cross sections are presented in Fig. 4(a) for the linear C-H-F geometry ($\alpha = 0°$). The charge-transfer process is clearly driven mainly by means of the nonadiabatic interactions in the vicinity of avoided crossings. The most important interaction corresponds to the radial coupling between the entry channel and the highest $2^1\Sigma^+\{C^+(1s^22s^22p)\,^2P + HF^+(^2\Sigma^+)\}$ exit channel, and effectively the corresponding partial cross section presents the highest values. The rotational effect, however, is quite significant for this system as this highest $\{C^+(1s^22s^22p)\,^2P + HF^+(^2\Sigma^+)\}$ exit channel may also be correlated with the entry channel by means of rotational coupling, and the partial cross section on the corresponding $2^1\Pi$ channel reaches values up to 7×10^{-16} cm^2. Different values of the HF distance r_{HF} have been considered in this linear approach in order to test the vibration effect for this collision system. The corresponding total cross sections are presented in Fig. 5(a). They show a regular increase when the vibration coordinate r_{HF} is reduced from 2.0 to 1.5 a.u., in agreement with the increase of the radial coupling matrix element rad23 between the entry channel and the $2^1\Sigma^+$ level displayed in Fig. 5(b). Such coupling is moved toward longer internuclear distances when the r_{HF} vibration coordinate decreases. In contrast, the radial coupling rad12 between $1^1\Sigma^+$ and $2^1\Sigma^+$ exit channels decreases with the r_{HF} vibration coordinate. The corresponding interaction becomes smoother and moves toward shorter internuclear distances. Such observations may directly link the nonadiabatic interactions between $^1\Sigma^+$ channels to the shape of the partial cross section sec32 as defined in Fig. 4(a). Two bumps may be observed for this partial cross section, one at lower collision energies, which may be attributed mainly to the avoided crossing between the entry channel and the $2^1\Sigma^+$ level. Such interaction increases for shorter r_{HF} values, as pointed out on the radial coupling matrix elements rad23 presented in Fig. 5(b), leading to an increase of the corresponding bump exhibited by the partial cross section sec32 shown in Figs. 4(a) and 4(b). On the other hand, the partial cross section sec32 exhibits a smoother bump at higher collision energies, which may be associated with the nonadiabatic interaction between $2^1\Sigma^+$ and $1^1\Sigma^+$ exit channels. Its shape becomes smoother for shorter values of the vibration coordinate r_{HF} as presented in Figs. 4(a) and 4(b), in agreement with the variation of the radial coupling matrix element rad12
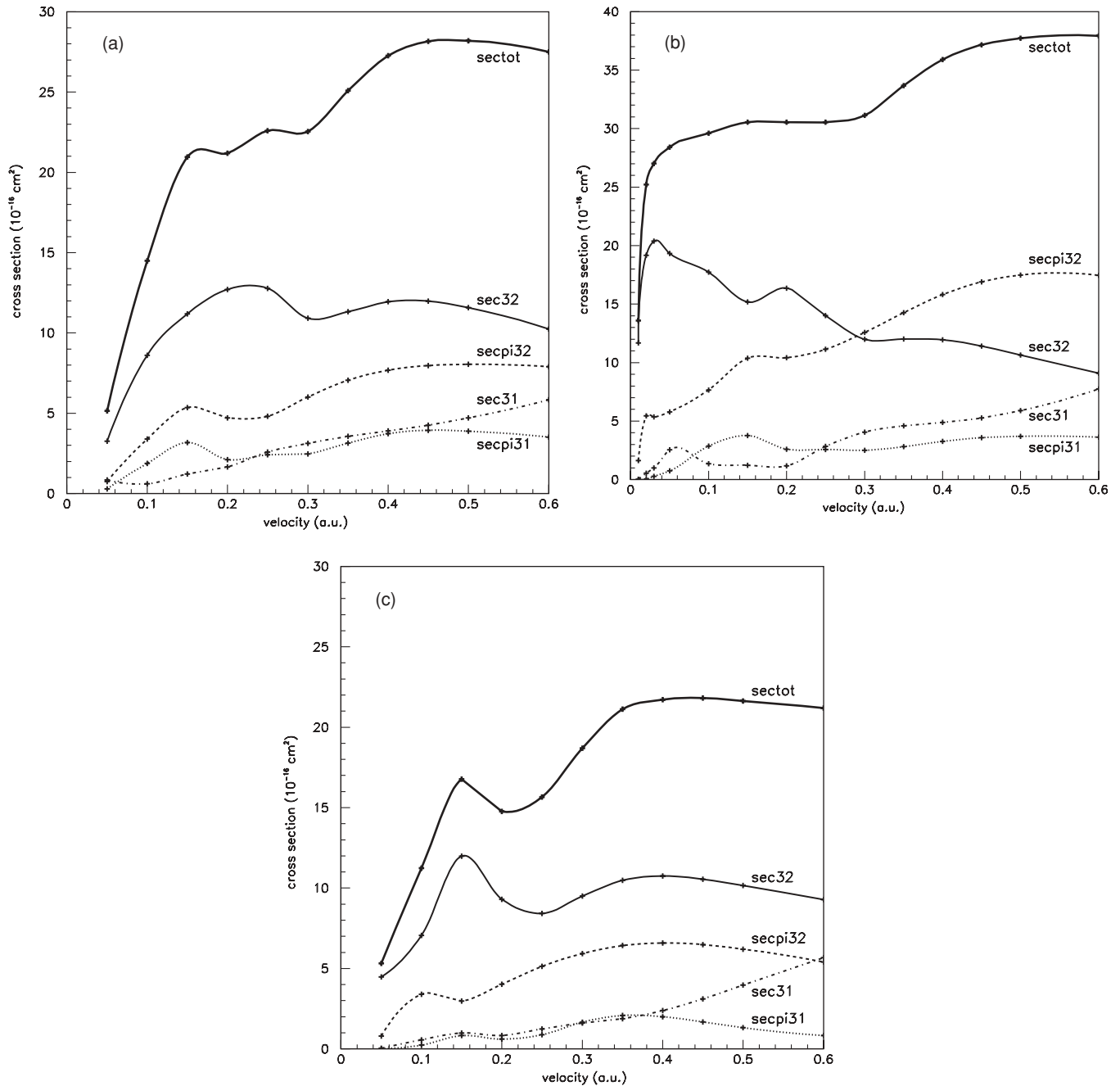
FIG. 4. (a) Total and partial charge-transfer cross sections for the C^{2+}-HF system at equilibrium, $\alpha = 0°$: sectot, total cross section; sec32, partial cross section on $^1\Sigma^+\{C^+(1s^22s^22p)\,^2P + HF^+(^2\Sigma^+)\}$; secpi32, partial cross section on $^1\Pi\{C^+(1s^22s^22p)\,^2P + HF^+(^2\Sigma^+)\}$; sec31, partial cross section on $^1\Sigma^+\{C^+(1s^22s^22p)\,^2P + HF^+(^2\Pi)\}$; secpi31, partial cross section on $^1\Pi\{C^+(1s^22s^22p)\,^2P + HF^+(^2\Pi)\}$. (b) Total and partial charge-transfer cross sections for the C^{2+}-HF system for the vibration coordinate $r_{HF} = 1.5$ a.u., $\alpha = 0°$ [same labels as in part (a)]. (c) Total and partial charge-transfer cross sections for the C^{2+}-HF system at equilibrium, $\alpha = 45°$ [same labels as in part (a)].

exhibited in Fig. 5(b). This analysis provides an interesting insight into the mechanism of the charge-transfer process with regard to the vibration of the molecular target. Anyway, no specific behavior is exhibited at very constrained HF geometry, as observed previously in the C^{2+}-OH collision system [5], and no first relaxation process may be expected for this system.

An estimate of the cross sections on the different vibrational levels v in $C^{2+} + HF_{(v=0)} \rightarrow C^+ + HF^+_{(v)}$ may be achieved in the sudden approximation method, assuming that the nuclear vibration and rotation periods are much longer than the

collision time. In such an approach, the capture probability between the vibrational levels $\chi_{v=0}$ for HF and χ'_v for HF^+, at a given distance r_{HF}, may be given by

$$P_{0v}(r_{HF}; b, v) = \sum_j \left| \int a_j(r_{HF}; b, v)\chi_0(r_{HF})\chi'_v(r_{HF})\,dr_{HF} \right|^2$$

for an impact parameter b and a velocity v. If one takes into account that the $\chi_0\chi'_v$ product exhibits a peaked feature, it is thus possible to approximate r_{HF} by its value at equilibrium
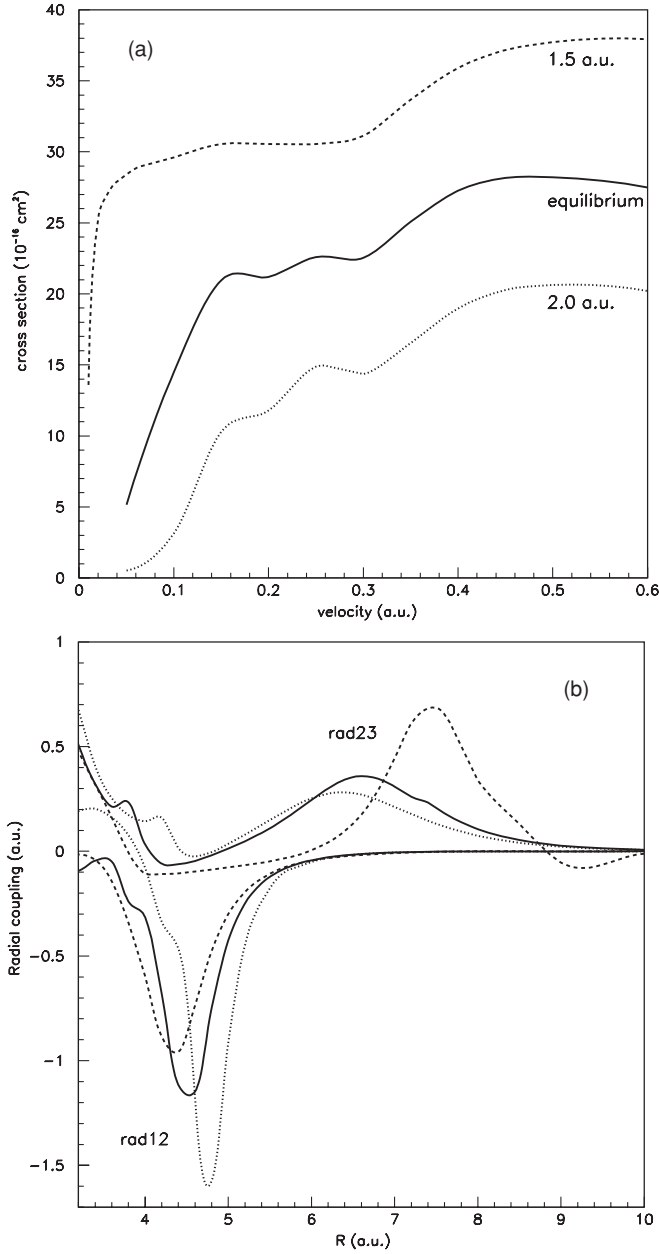
FIG. 5. (a) Total charge-transfer cross sections for the C^{2+}-HF system in the linear approach, $\alpha = 0°$, for different values of the vibration coordinate r_{HF}: dotted line, $r_{HF} = 2.0$ a.u.; solid line, $r_{HF} = 1.73836832$ a.u. (equilibrium); dashed line, $r_{HF} = 1.5$ a.u. (b) Radial coupling matrix elements between $^1\Sigma^+$ states of the C^{2+}-HF system in the linear approach, $\alpha = 0°$, for different values of the vibration coordinate r_{HF}. Upper curves, rad23; lower curves, rad12. Dotted line, $r_{HF} = 2.0$ a.u.; solid line, $r_{HF} = 1.73836832$ a.u. (equilibrium); dashed line, $r_{HF} = 1.5$ a.u.

and introduce Franck-Condon factors, neglecting the rotational modes. The probability in the centroid approximation may thus be expressed with regard to the corresponding electronic probability

$$P^{el}(r_{HF}; b, v) = \sum_j |a_j(r_{HF}; b, v)|^2$$

by

$$P^{C}_{0v}(r_{HF}; b, v) = P^{el}(r^{eq}_{HF}; b, v) F_{0v},$$

where F_{0v} is the Franck-Condon factor:

$$F_{0v} = \left[\int \chi_0(r_{HF}) \chi'_v(r_{HF}) dr_{HF} \right]^2.$$

By integration over the impact parameter, the cross section for the vibrational level v and collision velocity v is given in the Franck-Condon approximation by

$$\sigma^{FC}_{0v}(\mathbf{v}) = \sigma^{el}(r^{eq}_{HF}, \mathbf{v}) F_{0v},$$

where F_{0v} is the Franck-Condon factor between the HF and HF^+ vibration wave functions at equilibrium geometry for the vibrational level $v = 0$ and v, respectively.

Such an expression has been widely discussed and is certainly not satisfactory for low impact energies. However, it has been shown to provide a reasonable accuracy for impact energies greater than 500 eV/amu [32] and could be considered a first estimation, validated besides by the regular variation of cross sections with regard to the vibration coordinate r_{HF} as shown in Fig. 5(a). The vibration energy levels and Franck-Condon factors have been calculated in the anharmonic approximation using the program LEVEL 7.7 of R. J. Le Roy [33], valid for vibrational levels even near dissociation. The potential energy curves for HF and HF^+ have been determined at the CASSCF-MRCI level of theory by means of the MOLPRO code. The total charge-transfer cross sections in $C^{2+}(^1S) + HF_{(v=0)} \rightarrow C^+ + HF^+_{(v)}$ are given in Table II for a series of values of the collision velocities corresponding to impact energies between about 6 and 40 keV. The charge-transfer cross sections decrease very rapidly with increasing vibration number. They present significant values for $v = 0$, $v = 1$, and up to $v = 2$. The electron capture resulting in higher vibration levels of HF^+ is very weak.

The orientation of the projectile toward the molecular target has also been studied in detail for the $C^{2+} + HF$ system for geometries corresponding to specific values, about every $20°$, of the angle α from the linear geometry C-H-F ($\alpha = 0°$) to perpendicular ($\alpha = 90°$) and linear C-F-H geometry ($\alpha = 180°$). As pointed out in the previous paragraph, a strong evolution is observed in the potential energy curves when the angle α increases from the linear geometry $\alpha = 0°$ to nonlinear geometries, up to $\alpha = 90°$. Such evolution may be analyzed for chosen specific values $\alpha = 0°$, $45°$, $90°$, $135°$, and $180°$, in parallel with the total cross sections

TABLE II. Total cross sections for the $C^{2+} + HF_{(v=0)} \rightarrow C^+ + HF^+_{(v)}$ charge-transfer process (in 10^{-16} cm^2) for different velocities v (in a.u.).

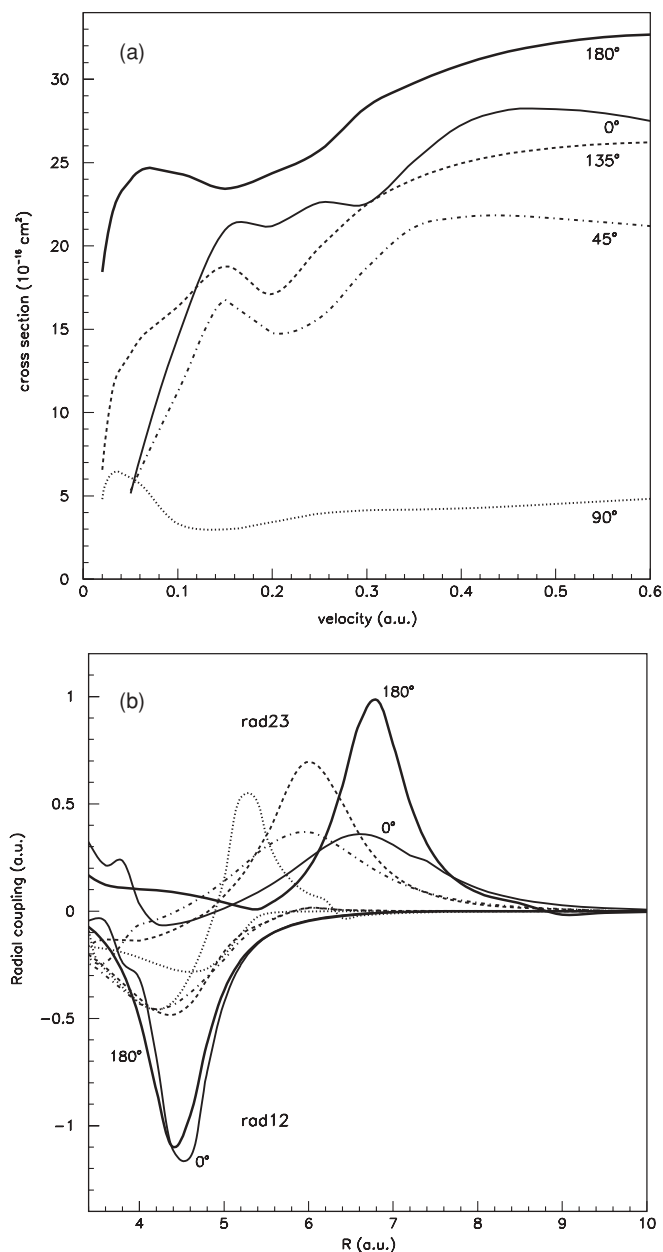|			v		
v	0.15	0.2	0.25	0.3	0.35
0	14.260	14.424	15.379	15.339	17.071
1	5.007	5.064	5.400	5.385	5.994
2	1.279	1.293	1.379	1.375	1.531
3	0.305	0.308	0.329	0.328	0.365
4	0.073	0.075	0.080	0.079	0.088

FIG. 6. (a) Total charge-transfer cross sections for the C^{2+}-HF system at equilibrium, for different orientations α from $0°$ to $180°$. Dotted line, $\alpha = 90°$; dot-dashed line, $\alpha = 45°$; dashed line, $\alpha = 135°$; thin solid line, $\alpha = 0°$; thick solid line, $\alpha = 180°$. (b) Radial coupling matrix elements between $^{1}\Sigma^{+}$ states of the C^{2+}-HF system at equilibrium for different orientations. Upper curves, rad23; lower curves, rad12. Dotted line, $\alpha = 90°$; dot-dashed line, $\alpha = 45°$; dashed line, $\alpha = 135°$; thin solid line, $\alpha = 0°$; thick solid line, $\alpha = 180°$.

presented in Fig. 6(a) and on the main radial coupling matrix elements displayed in Fig. 6(b). From cross-section results, it appears quite clear that the charge-transfer process is favored in the linear geometry. The collision with the fluorine atom ($\alpha = 180°$) is particularly efficient. In contrast, the charge-transfer process is markedly nonfavored in the perpendicular geometry corresponding to significantly lower charge-transfer cross sections. Such a result absolutely corroborates our previous studies on the $C^{2+} + OH$ and $C^{2+} + CO$ collision systems. In such collisions with heteronuclear

molecular targets, the charge transfer is always favored in a collinear approach toward the most electronegative atom, preferentially fluorine or oxygen rather than hydrogen for HF and OH, or carbon in the case of the CO molecular target. In our previous study on $C^{2+} + CO$ charge transfer, such a result was connected directly to the variation of the nonadiabatic interaction between the entry channel and the main exit channel characterized by the corresponding radial coupling matrix element [6]. The discussion is a bit more complex in the present case, as the cross sections may be related to simultaneous variations of two avoided crossings, the avoided crossing between the entry channel and the $2^{1}\Sigma^{+}\{C^{+}(1s^{2}2s^{2}2p)\,^{2}P + HF^{+}(^{2}\Sigma^{+})\}$ level corresponding to the radial coupling rad23 on one hand, and the avoided crossing between the $2\,^{1}\Sigma^{+}$ and $1\,^{1}\Sigma^{+}\{C^{+}(1s^{2}2s^{2}2p)\,^{2}P + HF^{+}(^{2}\Pi)\}$ exit channels characterized by the radial coupling rad12, on the other hand. Effectively, both rad23 and rad12 present a maximum for the linear geometry toward fluorine ($\alpha = 180°$). The radial coupling matrix element rad12 shows a simple behavior that is almost symmetric for both sides of the collision and significantly sharper in both collinear orientations. In contrast, the radial coupling matrix element rad23 is relatively smooth for the geometries corresponding to a collision with the hydrogen atom, in particular from $\alpha = 0°$ to $\alpha = 45°$. As previously pointed out in the vibration effect analysis, these two nonadiabatic interactions may be assigned to the two bumps of the partial cross section. The bump at lower energies assigned to the interaction between the entry channel and the $2\,^{1}\Sigma^{+}$ level clearly increases from linear $\alpha = 0°$ geometry to $\alpha = 45°$ geometry, as shown in Figs. 4(a) and 4(c). It is shifted toward lower energies in nonlinear orientations until the perpendicular geometry is obtained. The second bump, on the contrary, becomes smoother in connection with a lower nonadiabatic interaction between $1\,^{1}\Sigma^{+}$ and $2\,^{1}\Sigma^{+}$ exit channels. More generally, such nonadiabatic interactions driven by radial coupling matrix elements lead to lower partial cross sections from linear to perpendicular geometries. The values of the cross sections on $^{1}\Pi$ levels, in particular the $2\,^{1}\Pi\{C^{+}(1s^{2}2s^{2}2p)\,^{2}P + HF^{+}(^{2}\Sigma^{+})\}$ channel, on the contrary remain significant for every orientation of the projectile toward the target. This leads, globally, to a significant rotational effect, which follows from the values of the cross sections averaged over the different orientations presented in Table III. The averaged total cross sections increase from about 14×10^{-16} to 22×10^{-16} cm^{2} in the 3–100 keV collision energy range.

IV. CONCLUDING REMARKS

We have presented a theoretical treatment of charge-transfer processes induced by collision of the C^{2+} projectile ions on the HF molecule. The collision process is highly anisotropic: the charge transfer is favored in the linear approach with collision of the C^{2+} ion toward the fluorine atom, and, on the contrary, very significantly nonfavored in the perpendicular approach. An interesting insight into the more detailed mechanism of the process has been exhibited, with regard to the behavior of the collision system in different orientations, as well as for different values of the vibration coordinate r_{HF}. A clear correlation may be driven between the partial cross-section values and the nonadiabatic interactions shown by the molecular

TABLE III. Charge-transfer cross sections averaged over the different orientations for the C^{2+} + HF collision systems (in 10^{-16} cm^2).

Velocity (a.u.)	E_{lab} (keV)	sec32 $3\,^1\Sigma^+$-$2\,^1\Sigma^+$	secpi32 $3\,^1\Sigma^+$-$2\,^1\Pi$	sec31 $3\,^1\Sigma^+$-$1\,^1\Sigma^+$	secpi31 $3\,^1\Sigma^+$-$1\,^1\Pi$	sectot
0.05	0.75	7.04	2.68	0.48	0.34	10.54
0.1	3	8.41	3.99	0.86	0.96	14.22
0.15	6.75	8.78	4.79	1.04	1.48	16.10
0.2	12	8.75	5.31	1.24	1.33	16.64
0.25	18.75	8.56	6.04	1.76	1.53	17.89
0.3	27	8.13	6.97	2.19	1.81	19.10
0.35	36.75	8.18	7.68	2.52	2.10	20.51
0.4	48	8.25	8.10	2.89	2.25	21.49
0.45	60.75	8.16	8.22	3.38	2.24	22.01
0.5	75	7.94	8.15	3.96	2.15	22.20
0.6	108	7.37	7.64	5.25	1.96	22.23

system. A significant contribution of partial cross sections on $^1\Pi$ channels, in particular the highest $2\,^1\Pi\{C^+(1s^22s^22p)\,^2P +$ $HF^+(^2\Sigma^+)\}$ channel, driven by rotational coupling may be pointed out. Such remarks may be extended to provide a general understanding of charge-transfer processes in collision of ions with heteronuclear molecular targets.

[1] P. Sobocinski, J. Rangama, G. Laurent, L. Adoui, A. Cassimi, J.-Y. Chesnel, A. Dubois, D. Hennecart, X. Husson, and F. Frémont, J. Phys. B: At. Mol. Opt. Phys. **35**, 1353 (2002).

[2] G. Laurent *et al.*, Phys. Rev. Lett. **96**, 173201 (2006).

[3] R. E. Olson and C. R. Feeler, J. Phys. B **34**, 1163 (2001).

[4] M. C. Bacchus-Montabonel, Phys. Rev. A **59**, 3569 (1999).

[5] E. Bene, Á. Vibók, G. J. Halász, and M. C. Bacchus-Montabonel, Chem. Phys. Lett. **455**, 159 (2008).

[6] E. Bene, P. Martínez, G. J. Halász, Á. Vibók, and M. C. Bacchus-Montabonel, Phys. Rev. A **80**, 012711 (2009).

[7] M. C. Bacchus-Montabonel, M. Łabuda, Y. S. Tergiman, and J. E. Sienkiewicz, Phys. Rev. A **72**, 052706 (2005).

[8] M. C. Bacchus-Montabonel and Y. S. Tergiman, Phys. Rev. A **74**, 054702 (2006).

[9] M. C. Bacchus-Montabonel, Y. S. Tergiman, and D. Talbi, Phys. Rev. A **79**, 012710 (2009).

[10] B. D. Michael and P. D. O'Neill, Science **287**, 1603 (2000).

[11] F. Frémont, D. Martina, O. Kamalou, P. Sobocinski, J.-Y. Chesnel, I. R. McNab, and F. R. Bennett, Phys. Rev. A **71**, 042706 (2005).

[12] R. Cabrera-Trujillo, E. Deumens, Y. Ohrn, O. Quinet, J. R. Sabin, and N. Stolterfoht, Phys. Rev. A **75**, 052702 (2007).

[13] F. Alvarado, S. Bari, R. Hoekstra, and T. Schlatölter, J. Chem. Phys. **127**, 034301 (2007).

[14] J. de Vries, R. Hoekstra, R. Morgenstern, and T. Schlathölter, Phys. Rev. Lett. **91**, 053401 (2003).

[15] H. J. Werner and P. Knowles, computer code MOLPRO (version 2009.1) package of *ab initio* programs.

[16] D. E. Woon and T. H. Dunning Jr., J. Chem. Phys. **98**, 1358 (1993).

[17] M. S. Banna, B. E. Mills, D. W. Davis, and D. A. Shirley, J. Chem. Phys. **61**, 4780 (1974).

[18] K. P. Huber and G. Herzberg, in *Molecular Spectra and Molecular Structure IV. Constants of Diatomic Molecules* (Van Nostrand Reinhold, New York, 1979).

[19] R. W. Shaw Jr. and T. D. Thomas, Phys. Rev. A **11**, 1491 (1975).

[20] W. von Niessen, L. S. Cederbaum, W. Domcke, and G. H. F. Diercksen, Chem. Phys. **56**, 43 (1981).

[21] R. K. Chaudhuri, K. F. Freed, S. A. Abrash, and D. M. Potts, J. Mol. Struct. Theochem **547**, 83 (2001).

[22] NIST Atomic Spectra Database Levels Data, [http://physics.nist.gov/cgi-bin/AtData/main_asd]

[23] B. Lasorne, M. C. Bacchus-Montabonel, N. Vaeck, and M. Desouter-Lecomte, J. Chem. Phys. **120**, 1271 (2004).

[24] M. C. Bacchus-Montabonel, C. Courbin, and R. McCarroll, J. Phys. B **24**, 4409 (1991).

[25] R. J. Allan, C. Courbin, P. Salas, and P. Wahnon, J. Phys. B **23**, L461 (1990).

[26] B. H. Bransden and M. R. C. McDowell, in *Charge Exchange and the Theory of Ion-Atom Collisions* (Clarendon Press, Oxford, 1992), pp. 63–64.

[27] D. R. Bates and R. McCarroll, Proc. R. Soc. A **245**, 175 (1958).

[28] T. G. Winter and G. J. Hatton, Phys. Rev. A **21**, 793 (1980).

[29] L. F. Errea, L. Méndez, and A. Riera, J. Phys. B **15**, 101 (1982).

[30] F. Fraija, A. R. Allouche, and M. C. Bacchus-Montabonel, Phys. Rev. A **49**, 272 (1994).

[31] P. Honvault, M. C. Bacchus-Montabonel, and R. McCarroll, J. Phys. B **27**, 3115 (1994).

[32] L. F. Errea, J. D. Gorfinkiel, A. Macías, L. Méndez, and A. Riera, J. Phys. B **30**, 3855 (1997).

[33] R. J. Le Roy, LEVEL 7.7 computer program, [http://leroy.uwaterloo.ca].